

UNSTEADY COANDA FORCING FOR DRAG REDUCTION OF A BLUNT BODY

Yann Haffner, Jacques Borée, Andreas Spohn

Institut Pprime, UPR 3346, CNRS-Université de Poitiers-ENSMA
Futuroscope-Chasseneuil, France
yann.haffner@ensma.fr

Thomas Castelain

Univ Lyon, Université Claude Bernard Lyon I
École Centrale de Lyon, INSA Lyon,
CNRS, LMFA, UMR5509,
43 boulevard du 11 novembre 1918,
F-69100, VILLEURBANNE, France

ABSTRACT

We experimentally study the unsteady forcing of the turbulent wake of a three-dimensional blunt body for drag reduction purposes. The forcing is provided by pulsed jets coupled to small flush-mounted curved surfaces and affects the dynamics of the shear layer at separation from the trailing-edge of the model. The influence of various parameters (forcing frequency and amplitude, curvature radius r of the surfaces, free-stream velocity U_0) on the base drag reduction is scrutinized. The systematic analysis of the influence of each parameter provides key ingredients to identify proper scalings of the mechanisms involved. The flow reattachment and separation on the curved surfaces results in a boat-tailing of the wake leading to drag reductions up to 12% but is noticeably influenced by the unsteadiness of the forcing. Indeed for high frequencies of order $O(U_0/r)$, strong vortical coherent structures produced by the interaction of the pulsed jets and the separating shear layer favorize the interaction of the flow with the curved surfaces. The local curvature and pressure gradients across the separating shear layer are noticeably modified to result in an increase of the pressure drag reduction for a given energy input. Results point to the need of careful combination between forcing frequency and size of the curved surfaces to achieve all the potential of the unsteady Coanda effect in drag reduction.

INTRODUCTION

The flow around blunt geometries inducing massively separated turbulent flow with a low-pressure wake is of peculiar interest for the vehicle industry where aerodynamic form drag is the main energy consumption factor. The control of such flow by acting directly on the shear layers surrounding the recirculation region has been identified as a highly promising drag reducing method in recent years. Among the most efficient active control strategies for these wakes, steady (Freund & Mungal, 1994) and unsteady (Barros *et al.*, 2016) Coanda blowing have shown how it could lead to significant base drag reduction. This reduction oc-

curs through the possible reattachment process (Darabi & Wygnanski, 2004) over the surfaces involved in the Coanda effect (Wille & Fernholz, 1965). However, there is an important lack in the knowledge of the mechanisms involved in the unsteady Coanda effect and their impact on the turbulent wake drag.

In this study, we aim at identifying the fundamental differences between steady and unsteady Coanda blowing and their effect on the aerodynamic drag of blunt bodies. Wind-tunnel experiments with a blunt body are used where parametrized unsteady forcing coupled to small curved surfaces can be applied around the base. The results point to the need for a careful selection of combination between forcing frequency and curvature radius to achieve drag reductions up to 12%.

EXPERIMENTAL SETUP

The experiments presented in figure 1 are performed in a subsonic wind-tunnel whose test section dimensions are 2.4 m width and 2.6 m height with a turbulence intensity of about 0.5%. A blunt body similar to a square-back Ahmed body is placed on a false floor containing a 6-components aerodynamic balance to measure aerodynamic loads. The model of height $H = 0.3$ m, width $W = 0.36$ m and length $L = 1$ m is fixed at a ground clearance $G = 0.05$ m about five times greater than the on-coming false floor boundary layer thickness. The drag coefficient $C_x = F_x / (0.5\rho HWU_0^2)$, where F_x is the x -component of the aerodynamic load on the model, is measured with an incertitude of about 1%. Experiments are performed at various on-coming velocities U_0 corresponding to Reynolds numbers $Re_H = U_0H/\nu$ ranging from 4 to $8 \cdot 10^5$. The boundary layer at the upper rear edge at separation is fully turbulent with a momentum thickness measured by HWA of $\theta = 2.3$ mm at $Re_H = 5 \cdot 10^5$.

The pressure coefficient C_p at the back of the model is monitored using a series of tappings (detailed on figure 1(b)) linked either to a scanner (for time-averaged measurements) or to differential pressure sensors allowing, after

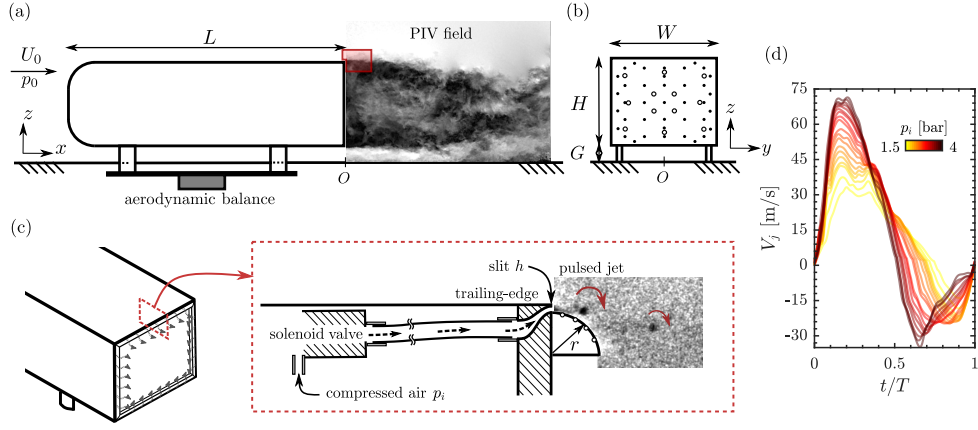


Figure 1. Experimental set-up. (a) Global set-up of the model in the wind-tunnel. (b) Rear view with the locations of the scanner taps (black dots) and unsteady pressure sensors taps (grey circles) for base pressure measurements. (c) Detailed sketch of the forcing system with additional pressure taps on the rounded surface. (d) Phase-averaged velocity profile at the center of the exit slit at $f = 975$ Hz with varying inlet pressure obtained from hot-wire measurements.

calibration, to perform time-resolved measurements with a bandwidth of 2 kHz.

Actuation is performed using pulsed jets of frequency f generated by an ensemble of solenoid valves supplied with compressed air and linked by semi-rigid tubing to diffusers ending in $h = 1$ mm-thick slits all around the base. In the present study all the slits are driven together in phase in order to perform a global forcing of the wake. The system is detailed in figure 1(c). Additional rounded surfaces of variable curvature radius $r = 5, 7, 9, 16h$ are placed flush to the slits in order to take advantage of a Coanda effect. In the remainder of this paper, the focus is put on $r = 9h$. 4 additional time-resolved pressure taps are located along these rounded surfaces. Forcing is driven at three very distinct frequencies $f = 0$ (steady), 350 and 975 (and 1050) Hz with variable inlet pressure p_i driving the forcing amplitude. These peculiar frequencies have been chosen as odd multiples of the fundamental Helmholtz acoustic resonance frequency of the tube mounting at which the velocity at the exit of a slit (given in figure 1(d) at $f = 975$ Hz) presents a simple peaking profile. In particular selected frequencies present similar velocity profiles to allow for a fair comparison of the physical effects of forcing. The amplitude of the forcing is characterized by a momentum coefficient C_μ defined as $C_\mu = d_c \cdot (s_j/S) \cdot (V_{j,max}^2/U_0^2)$, where d_c is the duty-cycle of the forcing, s_j (resp. S) the total cross-sectional area of the slits (resp. model), U_0 the on-coming velocity and $V_{j,max}$ the peak velocity during the forcing cycle. This amplitude is chosen based on the maximum velocity in order to more fairly compare steady and pulsed forcing.

2D2C PIV measurements are performed to obtain the velocity field in the wake. Both fields of view are located in the symmetry plane ($z = 0$). One of them spans the whole wake containing entirely the recirculating flow domain with a spatial resolution of about $0.004H$. The other one (depicted in red in figure 1(a)) focuses on the upper shear layer just after separation and enables highly spatially resolved measurements with a final spatial resolution of $0.16h$. For this FOV phase-locked measurements are performed using the forcing signal as a reference.

SCALINGS OF DRAG CHANGES

The focus is first put on the analysis of global drag changes in order to introduce the main peculiar effects which will be further investigated in the rest of the paper. To quantify the global drag changes, we introduce a base pressure parameter γ_p which is the ratio between the forced and unforced mean base pressure \bar{C}_{pb} averaged over all the base. Similarly, we introduce a pressure drag parameter γ_p^c defined in the same way as γ_p but taking into account in addition the pressure changes on the curved surfaces measured at the location of the 4 additional pressure taps. Assuming an homogeneous pressure distribution along the span of the curved surface, the corrected base pressure C_{pb}^c is given as

$$S C_{pb}^c = (S - S_{cs}) C_{pb} + S_{cs} \left\langle \sum_{i \in cs} C_p(\theta_i) \sin \theta_i \right\rangle \quad (1)$$

where $S_{cs} = 2(H + W)\pi r/2$ is the total surface of the curved surfaces, θ_i the angular position of the pressure taps on the curved surface from the exit slit, and $\langle \cdot \rangle$ denotes a spatial average. Only γ_p^c is presented for the sake of brevity but similar trends have been found for direct aerodynamic drag measurements. The evolution of γ_p with C_μ (figure 2) presents a strong dependence on the forcing frequency. Indeed, the amount of base pressure recovery is more sensitive to an increase in C_μ for high frequencies ($f = 975$ and 1050 Hz) than for moderate frequencies ($f = 350$ Hz). Steady forcing is even seen to be inefficient to reduce the pressure drag of the model. This points to a quantifiable coupling mechanism between the forcing frequency and the size of the curved surfaces. It is worth mentioning here that this coupling has been further evidenced with systematic curved surfaces size r variation, which is not shown here in a matter of conciseness. In addition, the trends of γ_p are fundamentally different between forcing frequencies as high forcing frequencies exhibit a saturation in base pressure recovery (around $C_\mu = 3 \times 10^{-2}$ at $\gamma_p = 0.78$ for $U_0 = 25$ m/s) which is absent for moderate forcing frequencies. This saturation regime is hypothesized to be the consequence of different mechanisms of interaction between pulsed jets and curved surfaces in the base drag reduction effect. At amplitude C_μ at which saturation occurs at $U_0 = 25$ m/s, the base pressure increases by 22% for $f = 1050$ Hz, which is 6% more than

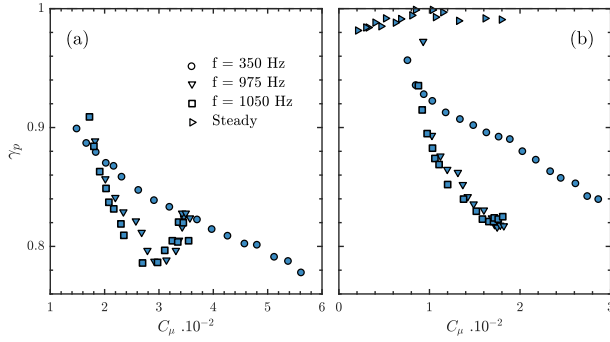


Figure 2. Base pressure changes γ_p for $r = 9h$ with forcing amplitude for studied frequencies : (a) $U_0 = 25$ m/s, (b) $U_0 = 35$ m/s. For steady forcing, because of the higher mass flow rates required by the forcing system, $U_0 = 20$ m/s to keep C_μ of comparable order of magnitude to that of pulsed forcing.

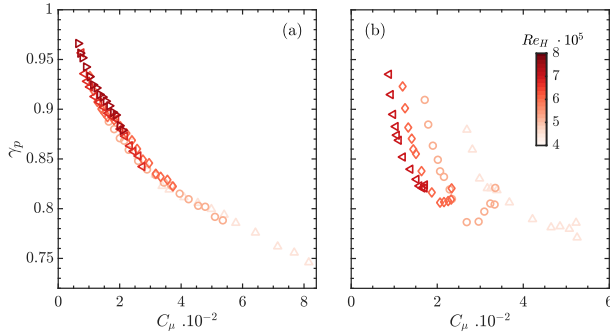


Figure 3. Re -dependence of base pressure changes γ_p for $r = 9h$: (a) $f = 350$ Hz, (b) $f = 1050$ Hz.

for $f = 350$ Hz, and is associated with a 12% drag reduction.

In an effort to find a convincing scaling of the base pressure changes, figure 3 presents the evolution of γ_p with the defined C_μ for changing Reynolds number Re_H (changes in Re_H are operated through changes of U_0 solely). For $f = 350$ Hz, C_μ seems to be the adequate scaling variable as all γ_p curves at different Re_H fall onto the same curve. Nevertheless it is not the case for the forcing at $f = 1050$ Hz where the curves at different Re_H are shifted and the saturation in γ_p doesn't occur at a fixed C_μ . The different mechanisms involved in the interaction between pulsed jets and curved surface is clearly evident from this observation. The discussion about a proper scaling in the latter case is enriched based on the detailed analysis of the wake in the following section.

In order to account for pressure variations on all parts of the base of the model, a corrected version of γ_p including the low pressure penalization (Chaligné, 2013) over the curved surfaces is presented in figure 4. The penalizing effect of the low pressure region created over the curved surfaces is seen from the increased values of γ_p^c compared to γ_p . The evolution of γ_p^c is highlighting even more the saturation in base pressure recovery occurring for high frequencies, thus suggesting the increased penalization from the curved surfaces for higher forcing amplitudes. It also shows that high frequency forcing is able to emulate other drag recovery mechanisms minimizing the negative effect due to attached flow around the curved surface.

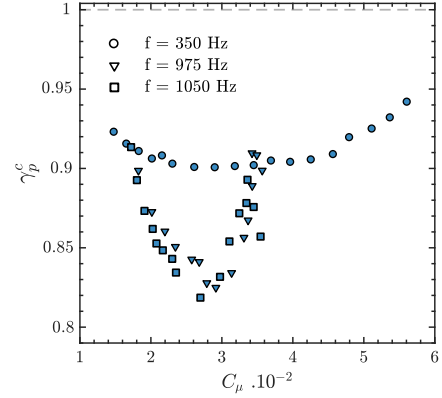


Figure 4. Base drag changes γ_p^c for $r = 9h$ and $U_0 = 25$ m/s with forcing amplitude.

UNSTEADY COANDA EFFECT MECHANISM

After having presented the global aerodynamic drag changes depending on forcing and identified an important coupling between forcing frequency and the size of curved surfaces, this section is focused on the detailed flow analysis in order to explain the global observations of the previous section.

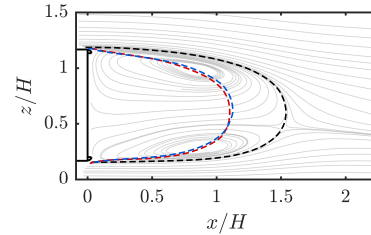


Figure 5. Wake separatrix for three cases at $U_0 = 25$ m/s : unforced flow (black), $f = 1050$ Hz around maximum base pressure recovery $C_\mu = 3 \times 10^{-2}$ (blue), and $f = 350$ Hz at equivalent forcing amplitude (red).

To get insights into the global changes of the wake under forcing, the wakes of two cases of interest ($f = 350$ Hz and $f = 1050$ Hz both at an amplitude $C_\mu = 3 \times 10^{-2}$ around the saturation in γ_p) are compared to the unforced one in figure 5. From a global point of view, both forced wakes are very similar in recirculation length and geometric aspect. Compared to the unforced wake, the forced ones are shortened because of a noticeable narrowing of the wakes directly linked to the base pressure recovery observed. As the global differences between both forced wakes are not obvious, the remaining of the analysis is focused on a finer local description in the vicinity of the model's trailing-edge.

As the pulsed jets are responsible for the modulation of the vorticity flux in the vicinity of separation, the wake dynamics are investigated through a phase-averaged description over the forcing cycle starting at the beginning of the blowing phase. The pressure dynamics on both the base of the model and along the curved surfaces are examined in figure 6 at $f = 1050$ Hz for increasing forcing amplitude below ($C_\mu = 2.1 \times 10^{-2}$), around ($C_\mu = 3 \times 10^{-2}$) and above ($C_\mu = 3.4 \times 10^{-2}$) the saturation in base pressure recovery. The evolution of the base pressure coefficient and of the pressure on the curved surface follows the velocity of the

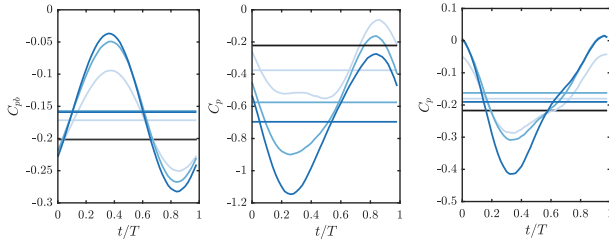


Figure 6. Phase-averaged evolution of the pressure for $f = 1050$ Hz at various forcing amplitudes $C_\mu = \{2.1, 3, 3.4\} \times 10^{-2}$ (respectively for darker shades of blue). Horizontal lines are the respective time-averaged values. From left to right : base pressure coefficient C_{pb} , and pressure at first and third locations from the slit on the curved surface (as indicated on figure 1(c)). Horizontal black lines indicate the unforced C_p .

pulsed jets obtained from the hot-wire calibration measurements. The base pressure coefficient C_{pb} peaks with V_j and is followed by a decrease both in line with the forcing amplitude. A mild saturation of the peaking amplitude of C_{pb} seems to take place whereas the amplitude of the decrease phase is constantly increasing. Over the curved surface, the pressure is evolving in phase opposition with the pulsed jets as a strong decrease in pressure is observed during the peaking phase of the forcing. This strong depression is related to the reattachment of the flow on the surface. When moving further downstream on the curved surface, the depression reduces but a greater relative gap between forcing amplitudes below and over the saturation amplitude appears and leads to a further pressure drag penalization at high C_μ . Both evolutions complement the saturation in base pressure recovery observed at high forcing amplitudes in figures 3(b) and 4.

In figure 7 the vorticity dynamics for both forced cases at $f = 350$ Hz and $f = 1050$ Hz at $C_\mu = 3 \times 10^{-2}$ around the saturation in base pressure recovery are presented. At $f = 1050$ Hz, the forcing cycle exhibits the formation of two main coherent structures of opposite vorticity, which are formed and convected downstream while interacting with the curved surface. The structure with negative vorticity denoted (I) in figure 7 appears to be formed mainly by the pinch-off of the separating boundary layer during the velocity peaking phase of the pulsed jets. The flux of vorticity contained in the boundary-layer upstream of separation is brutally perturbed by the begin of the blowing phase of the pulsed jets and rolls-up to form a structure of the apparent size of h . This structure is convected away and passes over the curved surface where it interacts with the reattachment process of the shear layer on the surface and downstream separation. The formation of this structure looks less clear at the medium frequency of $f = 350$ Hz. The circulation Γ_y of the vortices seen in figure 7 is defined as

$$\Gamma_y = \iint_S \omega_y(x, z) dx dz \quad (2)$$

where S is an arbitrarily defined surface containing the structure. The defined surface encompasses the high levels of $|\omega_y|$ around the peak vorticity, and the estimated circulation Γ_y is insensitive to variations in the definition of the surface as vorticity vanishes away from the structure. The evolution of the streamwise position of these structures

is presented in figure 8 against the non-dimensional time t/T . Contrarily to the $f = 350$ Hz case, the structure (I) can be unambiguously tracked over two forcing periods at $f = 1050$ Hz. This observation is of peculiar importance in the comparison of the timescale of the forcing and the convective timescale over the curved surface U_0/r . At the end of the forcing period, this structure has only attained about two times the streamwise extent of the curved surface. The higher density of presence of this additional structure in the vicinity of the curved surface with an induced velocity favourable to the curvature of and the pressure gradients across the separatrix appears to be the reason behind the efficiency difference in drag reduction between the two frequencies.

A second structure but of positive vorticity, denoted (II) in figure 7, is formed just after (I) and evolves with it as it is convected downstream. This structure, of increasing strenght with increasing forcing amplitude (as can be seen from figure 9), is formed due to the local velocity excess between the peaking jet velocity and the free-stream velocity. The strenght of this second structure is thus directly dependant on the velocity difference $V_j - U_\infty$ between the pulsed jet and the free-stream. The key role of this structure in the saturation mechanism of the unsteady Coanda effect is assessed through the tracking of both coherent structures (I) and (II) in figure 9. For forcing amplitudes below the saturation threshold, the circulation dynamics in the vicinity of the curved surface are dominated by (I) which results in a trajectory following the curved path imposed by the surface and in a beneficial effect for the local separating streamline curvature. Above the saturation threshold, the circulation dynamics are radically changed as (II) dominates. Its increased strenght induces an upward velocity (materialized by the arrow in figure 9) preventing the structure (I) from following the curved surface.

As the global view of the wake under forcing did not provide with fundamental changes between the different forcing frequencies, a further local investigation is performed in order to explain the differences observed in base pressure recovery and to link them to the vorticity dynamics in the separating shear layers. In figure 10 are provided the Reynolds stresses $u'v'$ for the three same cases as in figure 5 (unforced, $f = 350$ Hz and $f = 1050$ Hz at the same forcing amplitude $C_\mu = 3 \times 10^{-2}$ around the saturation). Their gradient are one main contribution to the pressure gradient according to the Reynolds-averaged momentum equations. As perceived from the tracking of coherent structures over the curved surface in figure 8, the increased time delay between the generation of successive velocity peaks at the lower frequency of $f = 350$ Hz results in an attachment and partial separation of the flow from the curved surface which is of higher amplitude. This is notably clear from the higher levels of $u'v'$ around the separation point on the curved surface. These imply important pressure gradients in the vicinity of the separation point which are penalizing the base pressure recovery by the low pressure induced near the curved surface. To give an explanation to the higher efficiency in base drag reduction of the higher forcing frequency, a reasoning on the curvature of the separating streamlines is built and presented in figure 11. Following the discussions of Sychev *et al.* (1982) and Bradshaw (1973), the mean normal pressure gradient across the separating streamline is related to the local non-dimensionalized streamline curvature κ , the tangential velocity u_s and the lo-

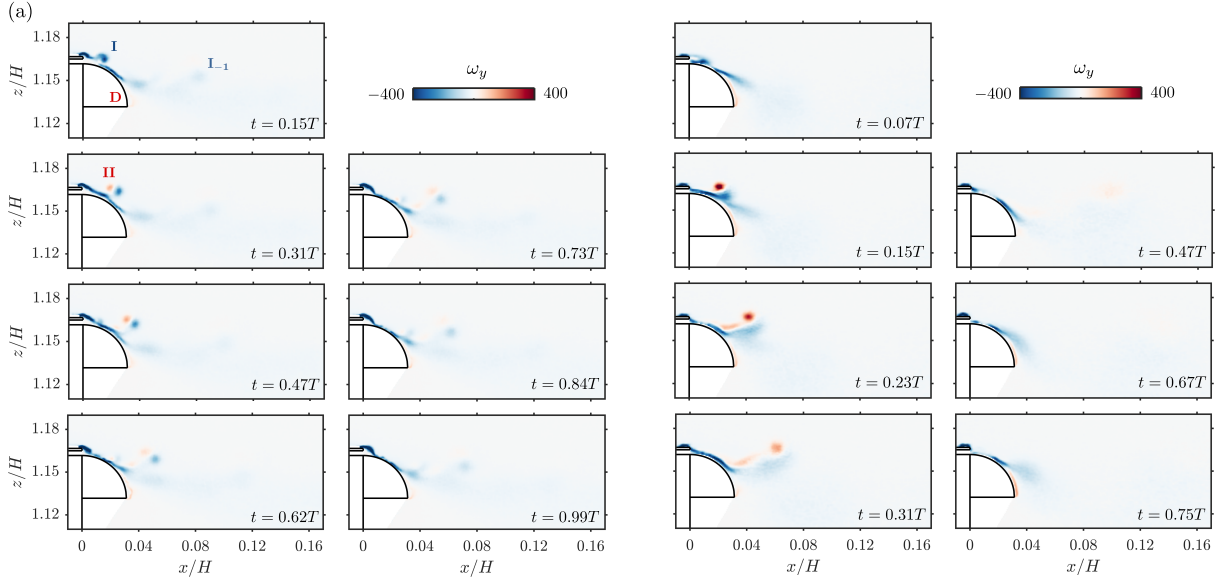


Figure 7. Phase-averaged evolution of the vorticity ω_y for (a) $f = 1050$ Hz around maximum base pressure recovery $C_\mu = 3 \times 10^{-2}$ (blue), (b) $f = 350$ Hz at equivalent forcing amplitude.

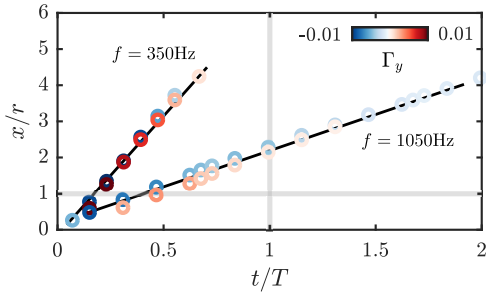


Figure 8. Streamwise position evolution of the tracked coherent structures identified in figure 7 for the two different forcing frequencies. Colormap quantifies the circulation Γ_y of the structures. Black lines give a linear trend of the position. Horizontal grey line is the streamwise position of the end of the curved surface.

cal variations of Reynolds shear stress by

$$C_{pn} = \frac{\partial C_p}{\partial n} = 2\kappa \bar{u}_s^2 - 2 \frac{\partial \overline{v'_n v'_n}}{\partial n} - 2 \frac{\partial \overline{u'_s v'_n}}{\partial s} \quad (3)$$

where s and n denote the coordinate respectively tangential and normal to the streamline. Here the normal gradient of the Reynolds shear stress acts only as a local pressure drop in the shear layer so that at first order only the mean curvature term and the longitudinal gradient of the Reynolds shear stress sets the pressure difference between the free-stream and the inner wake. The evolution of this term along the mean separating streamline is given in figure 11 for 4 representative cases : the unforced flow, the flow forced at $C_\mu = 3 \times 10^{-2}$ at $f = 350$ and 1050 Hz, and at higher C_μ at $f = 350$ Hz corresponding to a base pressure recovery equivalent to $f = 1050$ Hz. For a given base pressure recovery the separating streamline is significantly more deviated and results in a thinner wake at $f = 350$ Hz than at higher frequency where the streamline is more curved in the vicinity of the curved surface. Examination of the curvature and normal pressure gradient along the separating stream-

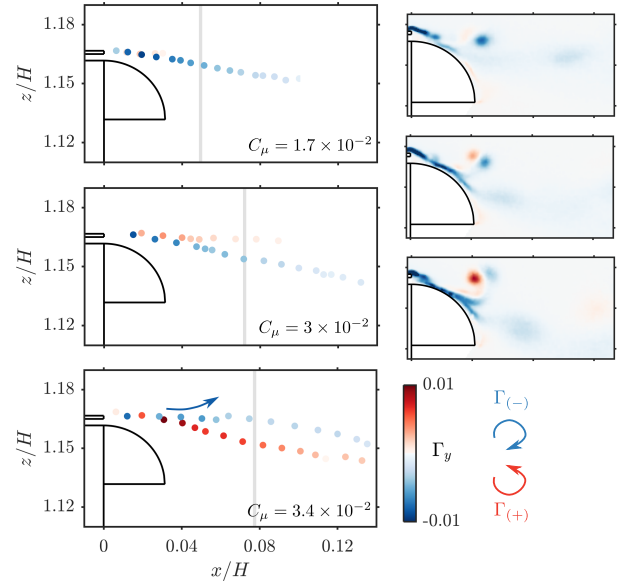


Figure 9. Tracking of the circulation of coherent structures from figure 7 for forcing at $f = 1050$ Hz at various amplitudes $C_\mu = \{1.7, 3, 3.4\} \times 10^{-2}$. The vertical grey lines denote the streamwise position of the structure (I) after one forcing cycle. Inserts on the right represents the corresponding vorticity field ω_y for each case around $t \sim 0.45T$ with the same colorscale as in figure 7.

line reveals a local curvature inversion near the base of the model responsible for the base pressure recovery. This curvature inversion is noticeably greater in the high frequency case with a concomitant evolution of the normal pressure gradient explaining the greater base pressure recovery observed. The influence of the coherent structures dynamics analysed previously appears thus of primary importance in the further changes of mean curvature observed.

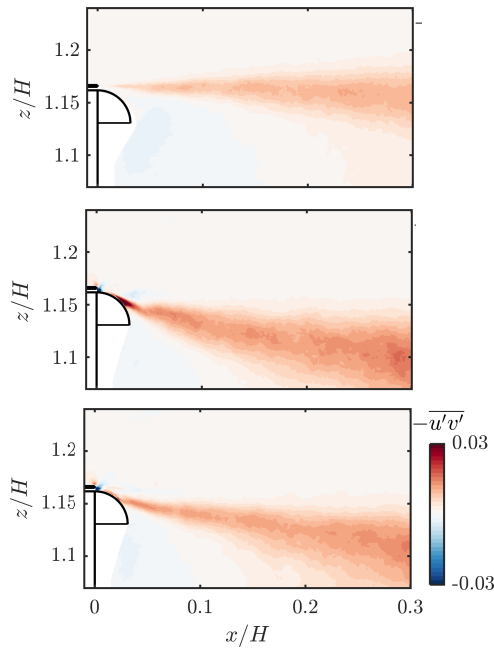


Figure 10. Evolution of $-\overline{u'v'}$ for unforced flow, $f = 350$ Hz at $C_\mu = 3 \times 10^{-2}$, and $f = 1050$ Hz at equivalent amplitude around maximum base pressure recovery.

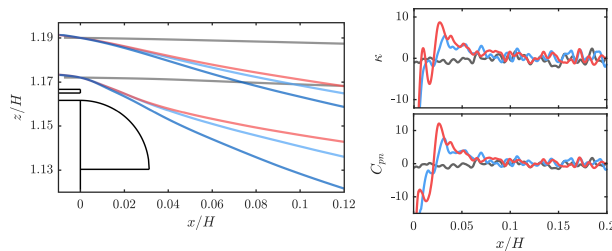


Figure 11. Streamlines, estimated local curvature κ and normal pressure gradient C_{pn} around the upper edge for different cases : unforced flow (gray), $f = 1050$ Hz around maximum base pressure recovery $C_\mu = 3 \times 10^{-2}$ (red), and $f = 350$ Hz at equivalent C_μ and at higher C_μ corresponding to equivalent base pressure recovery (shades of blue).

CONCLUSION AND OUTLOOK

The present paper has considered the forcing of the three-dimensional turbulent wake of a blunt body with pulsed jets coupled to small curved surfaces to reduce the pressure drag of the model. The flow reattachment and separation on the curved surfaces thanks to the pulsed jets results in a boat-tailing of the wake leading to drag reductions up to 12% but is noticeably influenced by the unsteadiness of the forcing. Indeed for high frequencies of order $O(U_0/r)$, strong vortical coherent structures produced by the interaction of the pulsed jets and the separating shear layer favorize the interaction of the flow with the curved surfaces. The local curvature and pressure gradients across the separating shear layer are noticeably modified to result in an increase of the pressure drag reduction for a given energy input. Results point to the need of judicious combination between forcing frequency and size of the curved surfaces to achieve all the potential of the unsteady Coanda effect in drag reduction. Indeed, additional investigations have shown the strong coupling between the radius of cur-

vature and the pulsed jets forcing frequency in the efficiency in drag reduction, pointing to the important role played by the unsteadiness. The scaling analysis partially discussed in the paper seems of fundamental practical importance for an industrial application on real vehicles where changing free-stream conditions and peculiar back body curvature will be of great influence. In addition, such a configuration associating time-dependent jets with frequencies of order $O(U_0/r)$ interacting with curved surfaces is of interest in a broad spectrum of applications and this study will be a first step in filling a gap in the literature.

ACKNOWLEDGMENT

The authors acknowledge the funding of the program Activ ROAD (ANR-15-CE22-0002) by the French Agence Nationale de la Recherche (ANR) and the financial support of Europe P.O. Feder and of Région Nouvelle Aquitaine CPER. They also warmly thank J.M. Breux and other partners from the program for invaluable assistance during the experiments and fruitful discussions.

REFERENCES

- Barros, D., Borée, J., Noack, B. R., Spohn, A. & Ruiz, T. 2016 Bluff body drag manipulation using pulsed jets and coanda effect. *J. Fluid Mech.* **805**, 422–459.
- Bradshaw, P. 1973 Effects of streamline curvature on turbulent flow. *Tech. Rep.*. DTIC document.
- Chaligné, S. 2013 Contrôle du sillage d'un corps non profilé. application expérimentale à une maquette simplifiée de véhicule industriel. PhD thesis, Ecole Centrale de Lyon.
- Darabi, A. & Wygnanski, I. 2004 Active management of naturally separated flow over a solid surface. part 1. the forced reattachment process. *J. Fluid Mech.* **510**, 105–129.
- Freund, J. B. & Mungal, M. G. 1994 Drag and wake modification of axisymmetric bluff bodies using coanda blowing. *J. Aircr.* **31**.
- Sychev, V.V., Ruban, A.I., Sychev, V.V. & Korolev, G.L. 1982 Asymptotic theory of separated flows .
- Wille, R. & Fernholz, H. 1965 Report on the first european mechanics colloquium, on the coanda effect. *J. Fluid Mech.* **23**, 801–819.